Chemical & Biomedical Engineering Faculty Publications

Chemical & Biomedical Engineering Department

10-25-2002

Compressive Properties of Zone-Directionally Solidified **β**-NiAl and Its Off-Eutectic Alloys With Chromium and Tungsten

R. Asthana
University of Wisconsin - Stout

R. Tiwari
Texas Instruments

Surendra N. Tewari
Cleveland State University

Original Citation

Asthana, R., Tiwari, R., , & Tewari, S. (2002). Compressive properties of zone-directionally solidified β-NiAl and its off-eutectic alloys with chromium and tungsten. Materials Science and Engineering: A, 336(1-2), 99 - 109.

Repository Citation

Asthana, R.; Tiwari, R.; and Tewari, Surendra N., "Compressive Properties of Zone-Directionally Solidified β-NiAl and Its Off-Eutectic Alloys With Chromium and Tungsten" (2002). *Chemical & Biomedical Engineering Faculty Publications*. 63.
https://engagedscholarship.csuohio.edu/encbe_facpub/63

Compressive properties of zone-directionally solidified β-NiAl and its off-eutectic alloys with chromium and tungsten

R. Asthana [a],*, R. Tiwari [b], S.N. Tewari [c]

[a] *Manufacturing Engineering, Technology Department, 326 Fryklund Hall, University of Wisconsin-Stout, Menomonie, WI 54751, USA*
[b] *300 mm CMP Process Team, Texas Instruments, 13011 TI Boulevard, Dallas, TX 75243, USA*
[c] *Chemical Engineering Department, Cleveland State University, Cleveland, OH 44115, USA*

1. Introduction

The ordered intermetallic compound β-NiAl is considered as an attractive material for structural applications in gas turbine engines because of its high melting point, low density, high modulus and excellent oxidation resistance. NiAl has been used as a coating material in aircraft engines, but in a bulk polycrystalline form, the material is extremely brittle, and its strength above about 773 K is very low. As NiAl exists over a wide range of stoichiometries, it is possible to utilize suitable alloying additions to NiAl to improve its mechanical properties [1,2]. For example, the alloying elements Ti, Nb, Ta, Mn, Cr, Co, Hf, W, Zr and B have been added to NiAl for increased resistance to compressive creep, with Nb and Ta being especially effective. Small additions of tungsten (0.2 at.%) to NiAl result in grain refinement in rapidly solidified (melt spun) ribbons; tungsten also inhibits grain growth during the subsequent hot consolidation, resulting in some improvement in crack resistance [2].

Microalloying of NiAl single crystals [3], martensitic transformation toughening [4], and ductile-phase toughening [5,6] by either directional solidification or deformation processing of ternary NiAl alloys have been shown to improve the low-temperature ductility and toughness of NiAl. For example, extrusion, rolling, and forging have been used for ductile-phase toughening of β-NiAl. Heat treatment of an extruded Ni–30Al–20Co alloy and a Ni–36Al alloy produced equiaxed β-NiAl grains containing a necklace of continuous γ′ at the grain boundaries, resulting in a slight improvement in the ductility (0.5%) over almost zero ductility of the alloy without the γ′ phase [7]. Ishida et al. [8] forged and rolled Ni–20Al–20Cr, Ni–25Al–

18Fe, Ni–15Al–65Fe and Ni–26Al–50Co alloys to obtain a uniform distribution of equiaxed β and γ grains with about 2–6% ductility at room temperature. Guha et al. [9] extruded a cast Ni–20Al–30Fe alloy to produce a fine equiaxed β-phase distributed in a β + γ′ eutectic. Depending upon the fineness of the γ′ phase, this alloy exhibited 8–22% ductility at room temperature. The ductility enhancement in systems toughened using the ductile-phase toughening approach has been attributed to inhibition of crack nucleation in the β-phase, and inhibition of crack growth due to plastic bridging by the ductile phase (crack bridging).

The first evidence of ductile-phase toughening of β-NiAl was provided by Tewari [5] in the directionally solidified (DS) Ni–34Fe–9.9Cr–18.2Al (at.%) alloy whose microstructure consisted of alternating lamellae of Ni-rich γ-phase and about 40% β-phase. This in situ composite exhibited 17% tensile elongation at room temperature with fracture occurring by cleavage of the β-phase which was sandwiched between ductile necked regions of γ-phase. Likewise, DS of Ni–30Al alloys has been shown [6] to lead to aligned rod-like γ′ (Ni$_3$Al) precipitates in a β-phase matrix, and DS of Ni–30Fe–20Al alloys yields aligned β-NiAl and γ/γ′ precipitates [6]. In both these cases, about 10% ductility was achieved as compared to near-zero ductility of stoichiometric NiAl at room temperature. Similar observations have been reported in DS NiAl(Mo) [10], DS NiAl(Cr,Mo) [10], and DS Ni–40Fe–18Al [11] alloys. For example, directional solidification of NiAl(Mo) and NiAl(Cr,Mo) alloys resulted in a marked improvement in fracture resistance; these alloys had a rod-like and a layered microstructure, respectively, with the layered structure yielding superior fracture resistance [10]. Similarly, Chen et al. [12] and Johnson et al. [13] performed DS on several ternary-NiAl alloys, and characterized the microstructure, fracture toughness and compressive creep behaviors.

The creep resistance and ductility at room temperature of the Ni–Al intermetallics (notably β-NiAl and Ni$_3$Al) depends upon the interlamellar spacing in the eutectic and the second phase morphology, both of which can be controlled by varying the growth speed during the DS [14,15]. Thus, Hirano and Mawari [14] found that the DS of Ni$_3$Al at 25 mm h^{-1} resulted in columnar grained single-phase Ni$_3$Al with 60% tensile ductility at room temperature. However, the same material grown above about 50 mm h^{-1} yielded lower ductility than the columnar grained Ni$_3$Al grown at the lower speed.

The DS of pseudo-binary eutectic compositions of NiAl containing elements such as Re, Cr, Mo [15] and others yields aligned α-phase which can greatly improve the strength. Similarly, off-eutectic compositions of NiAl with Cr are known to improve its creep strength. Thus, rupture life of NiAl single crystals (⟨110⟩ orientation) doubled (from 66.8 to 126.1 h) when chromium additions increased from 2 to 4 at.% [16]. A significant amount of strengthening in the NiAl(Cr) is provided by a high volume fraction of the fine α-Cr precipitates obtained through solution treatment. Dislocation networks form on the precipitate boundaries in both extruded and DS NiAl(Cr) alloys [17–19].

Most alloys utilizing the ductile-phase toughening concepts contain relatively large quantities of alloying elements which often adversely affect the high melting point, low density, and excellent oxidation resistance of β-NiAl, thus defeating the very purpose for which NiAl is considered an attractive high-temperature structural material. To avoid such deleterious effects of alloying, the present study utilized the smallest quantities of ternary solutes (chromium and tungsten) in NiAl, guided by the standard phase diagrams for the pseudo-binary NiAl–Cr and NiAl–W eutectic systems. These off-eutectic pseudo-binary alloys of NiAl with Cr and W were directionally solidified in the floating-zone mode, and the compressive properties of the DS alloys in the temperature range 300–800 K were investigated. The compressive properties of the DS alloys were compared to the properties of these alloys in the extruded state from an earlier work by the authors [17,18]. Limited results on the tensile test and fracture toughness measurements on selected DS alloys are also reported.

2. Experimental procedure

β-NiAl, and its pseudo-binary alloys with Cr and W were induction melted and chill cast under a protective argon atmosphere in a high purity copper mold to yield 14 cm long and 5 cm dia cylindrical bars. These bars were vacuum encapsulated in steel cans and extruded at 1400 K to an extrusion ratio of 32:1 for the NiAl and NiAl(W), and 16:1 for the NiAl(Cr). The extruded bars were chemically cleaned in an acidic solution and were used as feed material for directional solidification in the 'floating-zone' mode. The floating-zone DS is a crucible-less melting and solidification process that ensures relatively high purity levels in the grown material, a feature of considerable value to the processing of high-temperature intermetallics. The DS was carried out by creating a molten zone (0.6–0.8 cm long) in the feed material using a 30 kW RF generator and a copper flux concentrator, and traversing the melt zone at 11 mm h^{-1} (3 μm s^{-1}) to 60 mm h^{-1} (17 μm s^{-1}) over the length of the feed rod. A positive pressure (20 kPa) of ultrahigh purity Ar was maintained during the DS to suppress the loss of Al because of its high vapor pressure. A radiation pyrometer was used to control the temperature of the zone to within ± 6 K of the desired value.

The DS bars were centerless ground and machined to obtain compression test specimens (length: 1.25 cm, dia: 0.63 cm). The compression tests were performed in air at a strain rate of 1.74×10^{-4} s^{-1} in 300–800 K temperature range. The tensile testing of DS NiAl and NiAl(Cr) specimens was done at 300 and 800 K in air atmosphere using buttonhead specimens (0.3 cm gauge diameter, 3.0 cm gauge length) at a strain rate of 1.3×10^{-4} s^{-1}. The tensile test specimens were electro-polished prior to testing. A DS NiAl specimen was tested for its room temperature fracture resistance using a four-point bend test on notched bar specimen with the loading direction normal to the DS growth direction. The microstructure was examined using both optical and scanning electron microscopy (SEM). For the compression test specimens, the cracks originating at the specimen surface and propagating into the specimen interior were examined. The specimens were cut normal to the compression axis and polished using the standard metallographic procedures to examine the crack paths using optical microscopy. The fracture surfaces of the compression test specimens were examined using the SEM.

3. Results and discussion

3.1. Microstructure and chemistry

The chemical compositions of the alloys, determined using inductively coupled plasma emission spectroscopy, were (at.%): Ni–46Al, Ni–43Al–9.7Cr, and Ni–48.3Al–1W. The as-cast microstructure of the NiAl(Cr) (Fig. 1) shows β-NiAl dendrites and NiAl–Cr interdendritic eutectic. The solid-state diffusivities of solutes (Cr and W) are low which results in solute enrichment of the
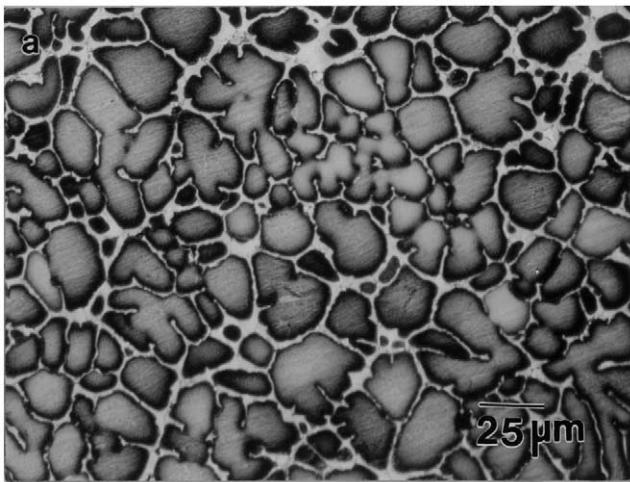

Fig. 1. The microstructure of a Ni–43Al–9.7Cr alloy cast in a copper mold showing β-NiAl dendrites and interdendritic NiAl–Cr eutectic.

residual liquid whose composition eventually reaches the eutectic composition (e.g. for the pseudo-binary NiAl–Cr alloys, the eutectic composition, C_E, is 33 at.% Cr). As a result, the eutectic solidifies in the last freezing interdendritic colonies as shown in the photomicrograph. Fig. 2(a) shows the longitudinal view of a zone DS NiAl bar and the solidified zones (rings) on the sample surface. The DS microstructures of NiAl and NiAl(Cr) alloys are shown in Fig. 2(b)–(e). The longitudinal view of a DS NiAl specimen (Fig. 2(b)) shows large columnar single-phase β grains oriented along the growth axis. The as cast β-NiAl exhibits an equiaxed grain structure with an average grain size of about 30 μm whereas in the DS material, grains are much coarser with the average β grain size in the order of 200–1100 μm (depending upon the growth speed). The DS NiAl(Cr) shows intercellular eutectic with a predominantly plate morphology of eutectic chromium, and a fine distribution of α-Cr precipitates (Fig. 2(c) and inset); the latter form in the matrix during specimen cooling after the DS because of low solubility of Cr in NiAl. The DS growth rate influences the structure; at low growth speeds (11 mm h^{-1} or 3 μm s^{-1}), the alloy NiAl(Cr) exhibits plane front solidification (shown in the top half of Fig. 2(d)) whereas at faster growth speeds (40 mm h^{-1} or 11 μm s^{-1}), the plane front breaks down into a cellular structure (bottom half of Fig. 2(d)) giving rise to intercellular eutectic. The NiAl(Cr) specimens for mechanical testing were grown at the higher growth speeds (40–60 mm h^{-1}) where a cellular microstructure is obtained. Whereas there were no major faults (e.g. banding) in the grown structures, the primary (β-NiAl) grains and the second-phase fibers (in the NiAl(Cr) and NiAl(W) alloys) were somewhat discontinuous, with the latter showing occasional branching or termination. It is anticipated that a better control of the zone DS process will yield a more uniform and consistent growth structure and mechanical properties.

3.2. Compressive strength

The load–displacement profiles for the DS NiAl(Cr) and NiAl(W) alloys revealed an abrupt drop in load at room temperature and at 500 K, but a gradual load drop at 600 and 800 K. In the case of DS NiAl, an abrupt drop in the load was observed at room temperature and at 600 K, but no abrupt drop in the load was observed at 500 and 800 K in this material. Table 1 summarizes the 0.2% compressive strength and fracture strain of DS NiAl alloys as a function of test temperature and Fig. 3 shows a plot of 0.2% compressive yield strength (CYS) versus temperature (data from Ref. [17,20,21] on extruded materials are also shown for comparison). Limited strength data generated from tensile tests on the DS alloys used in this study are given in Table 1.
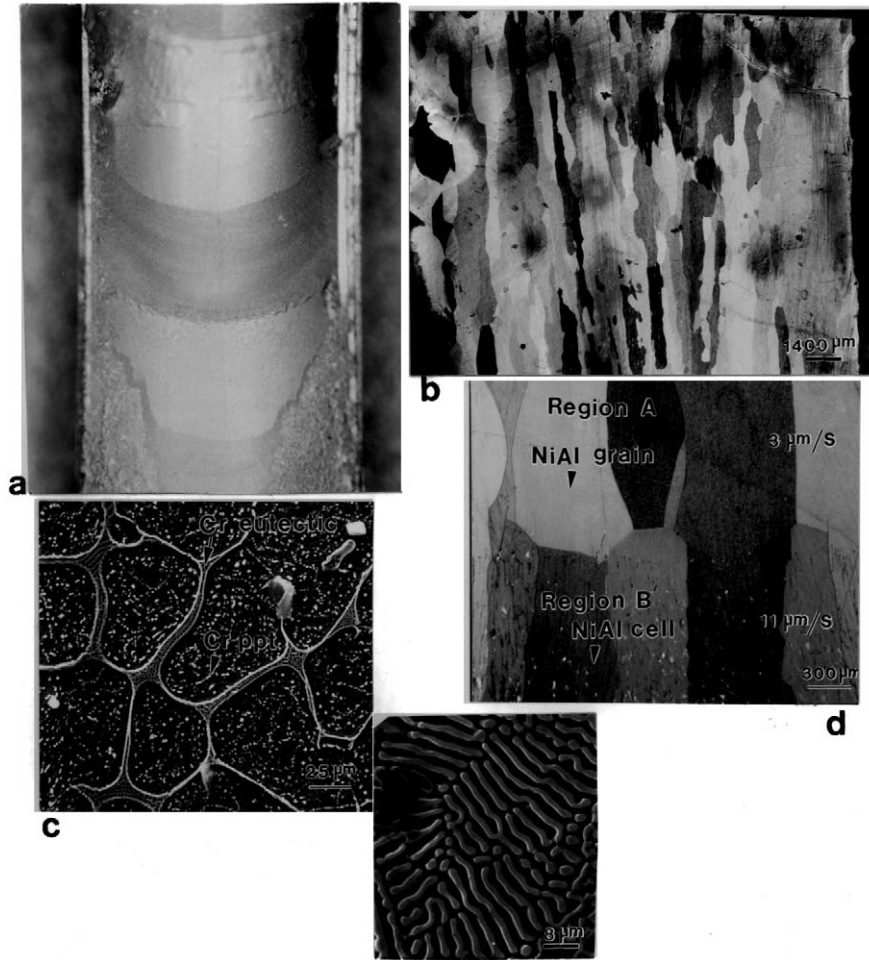
Fig. 2. (a) Longitudinal view of a zone directionally solidified (DS) NiAl bar showing the solidified zones (rings) on the sample surface; (b) longitudinal view of a DS NiAl specimen showing columnar β-NiAl grains; (c) transverse view of a DS NiAl(Cr) specimen showing the cellular NiAl structure with the chromium eutectic (inset) in the intercellular colonies and fine α-Cr precipitates within the β-phase matrix, and (d) longitudinal view of a DS NiAl(Cr) specimen showing breakdown of planar solidification front into cellular structure when the growth speed was increased from 3 to 11 μm s^{-1}.

The room temperature CYS of DS NiAl(Cr) (565.4 MPa) is about 30% greater than the CYS of DS NiAl (434.6 MPa). In contrast, the CYS of extruded NiAl(Cr) (895 ± 90 MPa) is about twice that of NiAl (451 ± 6 MPa). The CYS of DS and extruded NiAl at room temperature are nearly equal. The CYS of DS NiAl(W) (623.1 MPa) is higher than that of the DS NiAl (434.6 MPa), showing an increase of 44% as compared to about 30% increase with Cr additions. The CYS of DS NiAl(W), however, decreases more rapidly with increasing temperatures than the CYS of DS NiAl; at 800 K, the CYS of DS NiAl(W) (315.4 MPa) is slightly lower than that of the DS NiAl (356.3 MPa). Likewise, at 800 K, the CYS of DS NiAl(W) is somewhat lower than that of the NiAl(Cr), although the trend is reversed at lower temperatures. The room-temperature CYS of DS NiAl(W) (623 MPa) is largest of the three DS alloys investigated, although among the extruded alloys, NiAl(Cr) has the highest CYS (avg. 885 MPa) as shown by the data presented in Table 1.

The data presented in Table 1 also show that DS NiAl(W) has substantially higher CYS at all temperatures than the extruded NiAl(W). For example, at 300 K, the CYS of the DS NiAl(W) (623.1 MPa) is over 100% higher than the CYS of the extruded alloy (310 MPa). On the other hand, the NiAl(Cr) alloy shows a reverse behavior; the alloy in the extruded state has a significantly higher CYS than the same alloy under the DS condition. For example, the DS NiAl(Cr) has a CYS of 565 MPa at 300 K and 344 MPa at 800 K in contrast to the extruded material which has CYS of 885 MPa (avg) at 300 K and 518 MPa at 800 K (in fact, the CYS of the extruded alloy at 1000 K is comparable to the CYS of DS alloy at 800 K). Finally, the DS Ni–46Al alloy of the present study has a CYS of 435 MPa at 300 K which is comparable (albeit marginally lower) to the CYS of the extruded material (451 MPa) but significantly greater than the CYS (189 MPa) of the extruded Ni–50Al alloy used in Ref. [1]. The latter

difference arises from the effect of composition deviations from stoichiometry. Thus, a deviation from the ratio Ni/Al = 1 affects the mechanical properties because of the formation of nickel vacancies (Al-rich NiAl), or the substitutional nickel atoms on aluminum-rich sites (Ni-rich NiAl), leading to the strengthening of NiAl. Also noteworthy is the fact that the CYS (303 MPa) of a cast and hot extruded Ni–49.9Al alloy used in Ref. [20] at 300 K is appreciably greater than the CYS of 189 MPa given in Ref. [1] for a Ni–50Al alloy. Given that both these materials are stoichiometric in composition, the difference in their CYS is possibly due to the difference in the extrusion conditions, and the resulting grain sizes.

At the test temperature of 800 K, the DS Ni–46Al used in the present study has a CYS of 356 MPa whereas the same alloy in the extruded state has a CYS of 228 MPa [17]. As shown by the data of Table 1, the drop in the CYS of extruded NiAl with temperature in the range 300–800 K is more severe than that in the DS NiAl. On the other hand, for the NiAl(W) alloys, the decrease in the CYS in the temperature range 300–800 K is comparable for the extruded and the DS alloys (46–50% decrease), although the DS material retains significantly higher CYS at all temperatures. Similarly, for the NiAl(Cr) alloy, the decrease (39–42%) in the CYS from 300–800 K is about the same for both the DS and the extruded materials, although, unlike the NiAl(W) alloys, the extruded NiAl(Cr) alloy retained appreciably higher CYS at all temperatures as compared to the DS alloy.

In the DS NiAl material, alloying with tungsten gives strength advantage relative to unalloyed NiAl at temperatures below 800 K (at 800 K, the strength of NiAl(W) is slightly lower than that of NiAl). On the other hand, chromium alloying of DS NiAl appears to

Table 1
Mechanical properties of DS and extruded NiAl, NiAl(W) and NiAl(Cr) alloys

Test	Material [Ref.]	Temperature (K)	0.2% CYS or YS (MPa)	UCS or UTS (MPa)	Compressive fracture strain (%)
Compression	DS NiAl	300	434.6	564.8	7.33
Compression	DS NiAl	500	243.6	389.2	8.72
Compression	DS NiAl	600	600.0	807.9	5.98
Compression	DS NiAl	800	356.3	384.6	>5.07
Compression	DS NiAl(W)	300	623.1	820.5	9.80
Compression	DS NiAl(W)	500	523.1	882.6	9.96
Compression	DS NiAl(W)	600	666.7	1044.5	12.89
Compression	DS NiAl(W)	800	315.4	504.4	11.43
Compression	DS NiAl(Cr)	300	565.4	–	16.6
Compression	DS NiAl(Cr)	500	356.0		16.3
Compression	DS NiAl(Cr)	600	351.7	–	19.8
Compression	DS NiAl(Cr)	800	344.3	–	39.8
Compression	Extr. NiAl [20]	300	303	–	2.8
Compression	Extr. NiAl [20]	800	48	–	–
Compression	Extr. NiAl [20]	1100	39	–	–
Compression	Extr. NiAl [21]	673	291.6	–	–
Compression	Extr. NiAl [21]	973	208.3	–	–
Compression	Extr. NiAl [21]	1273	41.7	–	–
Compression	Extr. NiAl [17]	300	450	–	20
Compression	Extr. NiAl [17]	500	355	–	18
Compression	Extr. NiAl [17]	600	315	–	21
Compression	Extr. NiAl [17]	800	228	–	–
Compression	Extr. NiAl(Cr) [17]	300	1000, 860, 795	–	16
Compression	Extr. NiAl(Cr) [17]	500	975	–	17.4
Compression	Extr. NiAl(Cr) [17]	600	720	–	17.9
Compression	Extr. NiAl(Cr) [17]	800	518	–	28
Compression	Extr. NiAl(Cr) [17]	1000	330	–	–
Compression	Extr. NiAl(W) [17]	300	305, 310	–	25
Compression	Extr. NiAl(W) [17]	500	270	–	29
Compression	Extr. NiAl(W) [17]	600	240	–	38
Compression	Extr. NiAl(W) [17]	800	170	–	44
Compression	Extr. NiAl(W) [17]	1000	130	–	–
Tension	DS NiAl	800	194	239.2	2.94
Tension	DS NiAl(Cr)	800	300	313	0.28
Tension	Extr. NiAl [17]	800	253	352	6.3
Tension	Extr. NiAl(Cr) [18]	800	446	583	2.95

CYS, compressive yield strength; UCS, ultimate compressive strength; TYS, tensile yield strength; UTS, ultimate tensile strength.
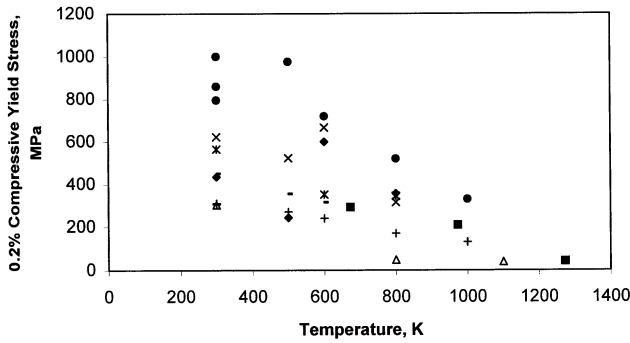
Fig. 3. Compressive yield stress (CYS) versus test temperature data for NiAl and selected ternary NiAl alloys from the present study. Also shown are the data from Refs. [7–9]. (◆), DS NiAl; (×), DS NiAl(W); (★), DS NiAl(Cr); (●), extruded NiAl(Cr) [7]; (—), extruded NiAl [7]; (+), extruded NiAl(W) [7]; (△), extruded NiAl [8]; and (■), extruded NiAl [9]. The strain rates during the compression tests were: 1.74×10^{-4} [7]; 8.5×10^{-4} [8], and 10^{-4} s^{-1} [9].
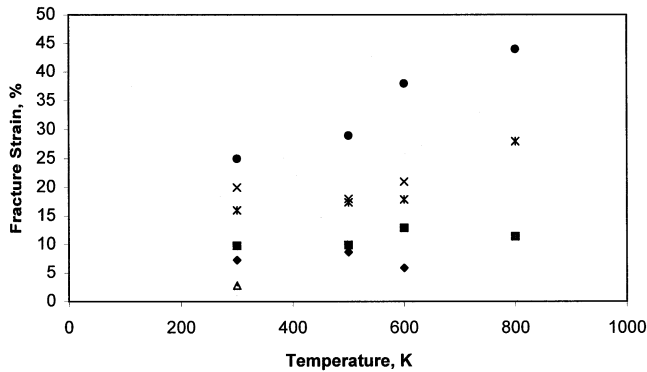

Fig. 4. Compressive fracture strain versus test temperature for the DS NiAl and DS NiAl(W) alloys. Also shown are the compressive strain data for extruded alloys from [7,8]. Legend—(●), extruded NiAl(W) [7]; (★), extruded NiAl(Cr) [7]; (×), extruded NiAl [7]; (△), extruded NiAl [8]; (◆), DS NiAl; and (■), DS NiAl(W).

provide strength advantage only at room temperature; at higher temperatures, unalloyed NiAl possesses higher strength. These trends in the extruded material are, however, different as documented in Ref. [17]. Tungsten alloying of NiAl does not yield any strength advantage over unalloyed NiAl in the extruded state up to 800 K; the unalloyed material retains a higher CYS at all temperatures (although W alloying improves ductility). On the other hand, the extruded NiAl(Cr) has a much greater strength at all temperatures than unalloyed NiAl in the extruded state. Thus, chromium alloying appears to be beneficial to strengthening of NiAl at all test temperatures (in the DS material, it was advantageous only at room temperature). Limited microhardness measurements (Knoop hardness, 300 g load) at room temperature on the DS Ni–46Al and DS Ni–43Al–9.7Cr alloys used in the present study indicate that the DS NiAl specimens (410 KHN) are somewhat harder than the DS NiAl(Cr) (340 KHN)

specimens which is related to the larger fracture strains (Table 1) of DS NiAl(Cr) (16.6%) than the DS NiAl (7.33%).

Table 1 also shows that the CYS of the DS alloys is greater than the tensile yield strength of these alloys. Thus, the CYS at 800 K of the DS NiAl and DS NiAl(Cr) are 356 and 344 MPa, respectively, whereas the tensile yield strengths are 194 and 300 MPa, respectively. A similar behavior was observed by Tiwari et al. [17,18] in the extruded alloys of the same composition, in the extruded stoichiometric Ni–50Al by Bowman et al. [22], and in NiAl–0.5Fe by Matsugi et al. [23]. Whereas the difference between the compressive and tensile yield strengths at 800 K for the extruded NiAl is insignificant [17], it is quite significant in the DS materials (over 100 MPa for the NiAl and 44 MPa for the NiAl(Cr)). This behavior is similar to the Bauschinger effect, which is attributed to the interaction between mobile dislocations and dislocation barriers. When the direction of loading is reversed, the pre-existing dislocations in the vicinity of dislocation tangles (created by the previous deformation) move at a stress lower than that required for the previous loading.

3.3. Compressive fracture strain

The compressive fracture strain was defined as the total strain when a drastic drop in the compressive stress occurred due to specimen fracture during testing. The data presented in Table 1 (and plotted in Fig. 4) show that the fracture strain of NiAl(W) is higher than that of the NiAl at all temperatures, and is in the range 9.8–12.9%, indicating an increase of about 30–116% with respect to unalloyed NiAl. This is qualitatively similar to the behavior observed for extruded NiAl and NiAl(W) alloys in Ref. [17].

The higher compressive fracture strain of the DS NiAl(W) than for the DS NiAl in the temperature range 300–800 K suggests the ductile-phase toughening potential of NiAl by tungsten alloying. Note, however, that the fracture strains of extruded NiAl(W) from Ref. [17] are appreciably greater (three-to-six times) at all temperatures than the fracture strains of the DS NiAl(W), although the CYS is higher for the DS material at all test temperatures than for the extruded material. Similarly, the fracture strain of the unalloyed extruded NiAl is about two-to-three times greater than the fracture strain of the DS material. On the other hand, the 0.2% CYS of the DS and extruded NiAl are similar at room temperature but at 600 and 800 K, the DS material exhibits higher CYS than the extruded NiAl.

The DS NiAl(Cr) possesses higher fracture strains (about twice) compared to the DS NiAl at 300 and 500 K. But at 600 and 800 K, there is a large increase in the fracture strain of the DS NiAl(Cr) compared to the DS

NiAl. Thus, at 800 K, the DS NiAl(Cr) has a fracture strain of ~40% compared to about 5% for the DS NiAl at the same temperature (Table 1). There is, therefore, a substantial gain in the ductility of the DS material due to chromium alloying of NiAl, and the strength of chromium alloyed DS NiAl is larger than or comparable to that of the DS NiAl (except at 600 K, where the DS NiAl has a much greater CYS than the DS NiAl(Cr)). In the extruded state, chromium alloying of NiAl only marginally improves the ductility [17], although the CYS increases substantially. Thus, it appears that chromium additions to create a dual-phase NiAl-based microstructure by directional solidification will be beneficial to both the strengthening and ductility enhancement of β-NiAl. In fact, chromium alloying is known to improve the fracture toughness of NiAl; the fracture toughness of eutectic NiAl(Cr) (about 18–21 MPa $\sqrt{}$m) is significantly greater than that of the poly-crystalline NiAl (about 4–6 MPa $\sqrt{}$m) and single crystal NiAl (~8 MPa $\sqrt{}$m).

3.4. Fractography

The fractography of DS NiAl compression test specimens showed mainly intergranular failure at room temperature (Fig. 5(a)), and a transgranular failure at 800 K (Fig. 5(b)). The DS NiAl(Cr) at room temperature showed a mixed mode failure (Fig. 6((a) and (b)) although the crack path was predominantly intergranular, and at 600 K, a predominantly intergranular failure (Fig. 6(c)) was observed. At room temperature, the DS NiAl(Cr) seems to have fractured by ductile tearing of the soft NiAl–Cr eutectic colonies and by transgranular cleavage of the β-NiAl grains. The somewhat dimpled fractured surface (Fig. 6(b)) of the DS NiAl(Cr) at room temperature is caused presumably due to pull-out of eutectic chromium in contrast to the predominantly

sharp-faceted cleavage fracture surface (Fig. 5(a)) of the DS NiAl due to decohesion of the grain boundaries. It is likely that in the DS NiAl(Cr), the β-grains deform and fractures before the yield strength of chromium is exceeded. At 800 K, the DS NiAl(Cr) showed almost completely intergranular failure (Fig. 6(d)) with the crack propagating through the intercellular eutectic regions. Finally, the DS NiAl(W) at room temperature showed a clear evidence of crack deflection by the tungsten precipitates (Fig. 7(a)) and the failure was transgranular (Fig. 7(b)).

The fracture surface of the room temperature tensile test specimen for the DS NiAl(Cr) is shown in Fig. 8(a)–(c) at three different magnifications. Considerable plasticity is evident from the appearance of the fractured surface, which agrees with the higher (16.6%) fracture strain of the material. The fracture surface of the DS NiAl tensile specimen tested at 800 K (Fig. 8(d)) shows transgranular failure.

3.5. Fracture resistance

The modulus of rupture (MOR) for the DS NiAl was measured using a four-point bend test on a notched specimen at room temperature. The MOR for this material was 503–520 MPa. This value is larger than the MOR of DS NiAl–40V (336 ± 37 MPa) reported by Johnson et al. [13] (the literature value of MOR of β-NiAl could not be found for comparison). The fracture surface of the DS NiAl specimen from the bend test (Fig. 9(a)) shows mainly transgranular fracture with sharp cleavage facets.

A preliminary test of fracture resistance to compressive deformation is provided by the cracking behavior around micro-indentations. Fig. 9((b) and (c)) show micro-indentations in a DS NiAl specimen and in a powder-processed β-NiAl specimen (a powder-pro-

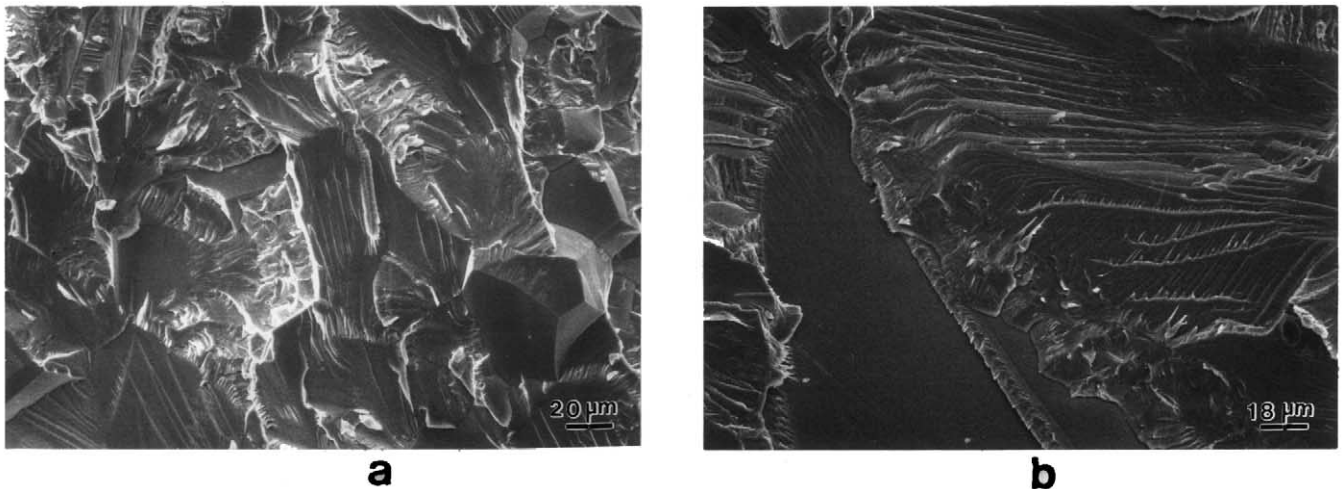a   b

Fig. 5. Photomicrographs showing fracture surfaces of compression tested DS Ni–46Al at (a) room temperature, and (b) at 800 K.
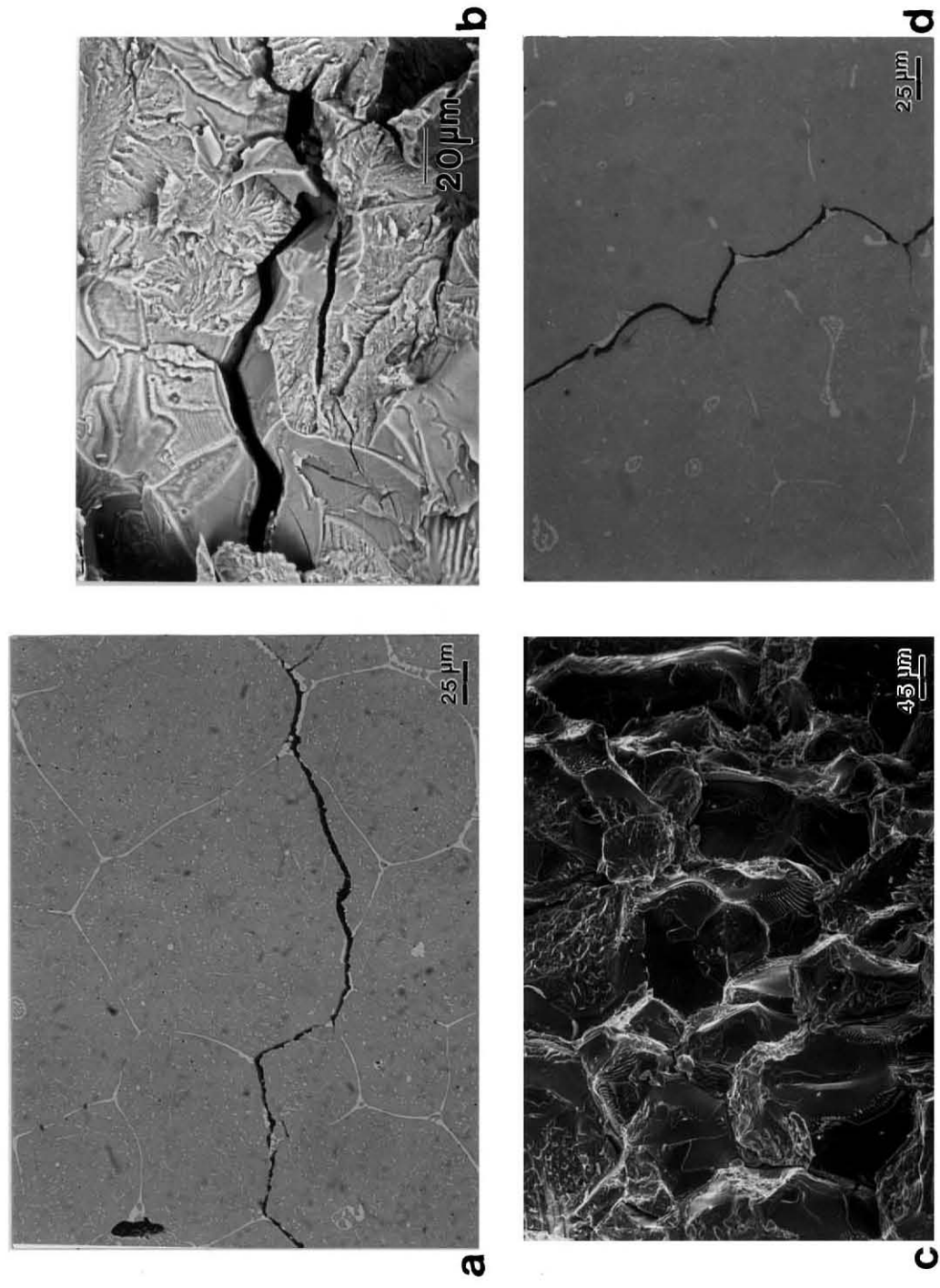
Fig. 6. Photomicrographs of fracture path and fracture surface in compression test specimens of DS Ni–43Al–9.7Cr tested at (a) and (b) room temperature; (c) at 600 K, and (d) at 800 K.
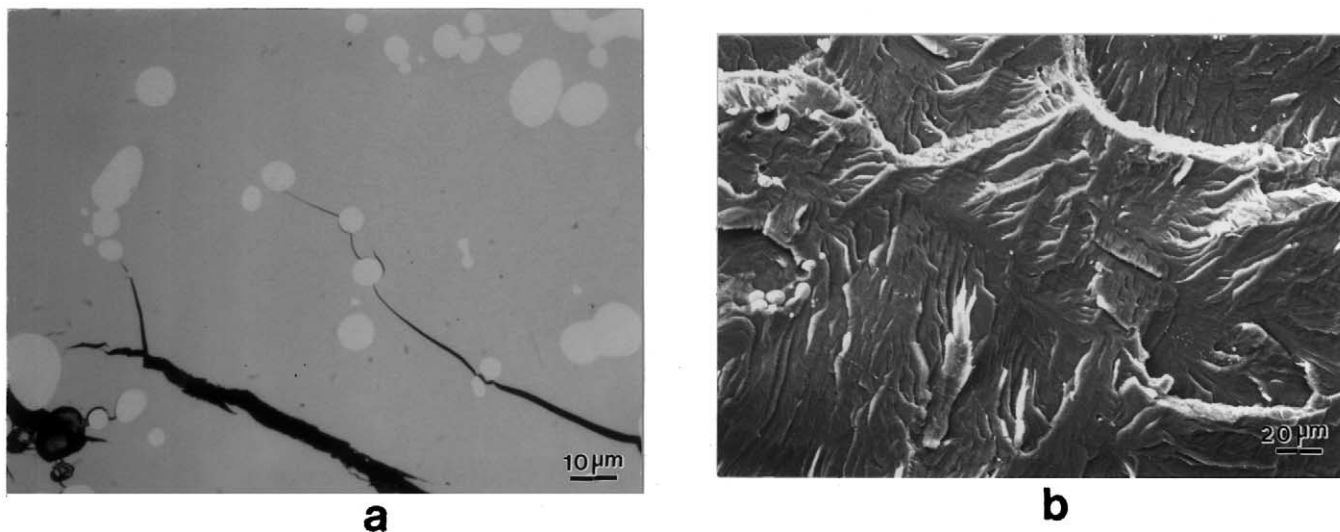
Fig. 7. Photomicrographs of compression tested DS Ni–48.3Al–1W specimen showing (a) crack deflection by tungsten precipitates, and (b) SEM view of the fracture surface.
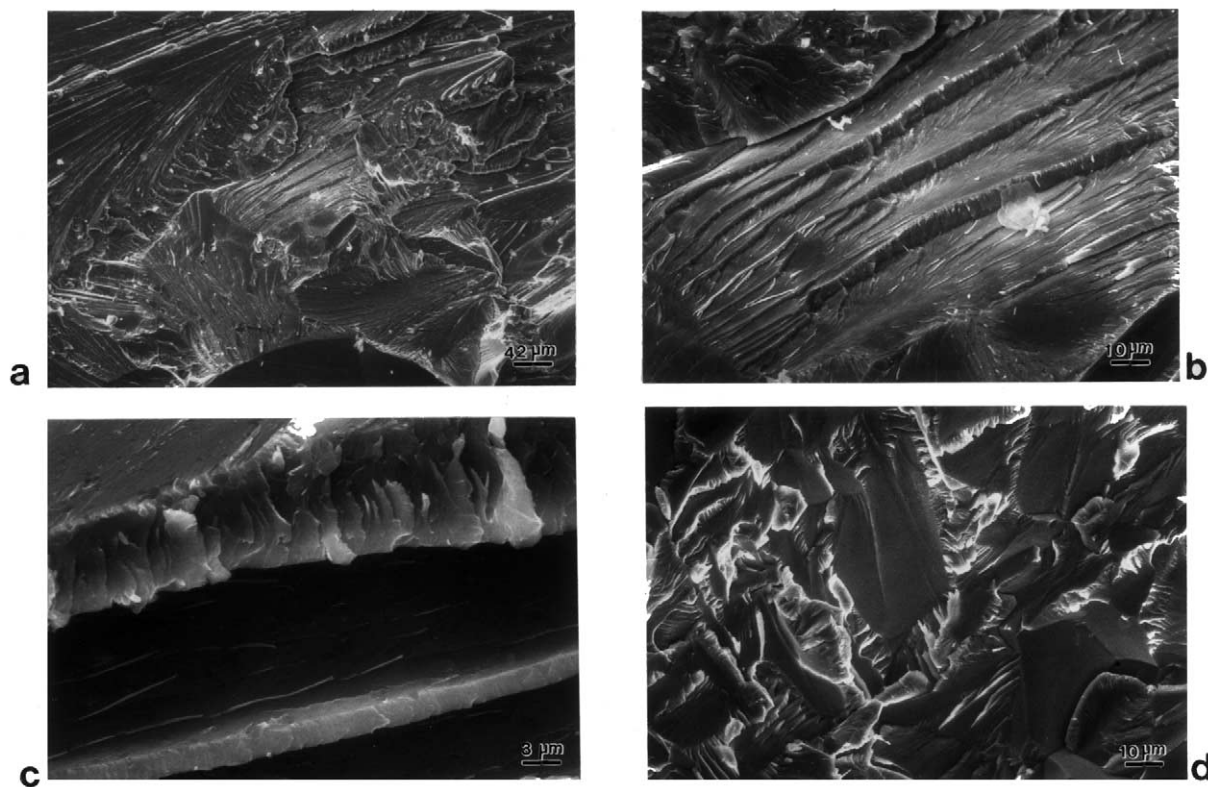

Fig. 8. SEM views (a)–(c) of fracture surface in a room-temperature tensile test specimen of a DS Ni–43Al–9.7Cr alloy, and (d) fracture surface in a room-temperature tensile test specimen of a DS Ni–46Al alloy.

cessed β-NiAl specimen also served as a feedstock for the subsequent DS). The low fracture toughness of the powder-processed material is evident from the matrix cracking around the indentation (Fig. 9(b)). In contrast, the DS material does not show any ma-

trix cracking in the vicinity of the indentation (Fig. 9(c)), suggesting that the alloy is not brittle under compressive loading, and possesses a higher fracture toughness under the directionally solidified condition.

4. Conclusions

The dual-phase structures created by directional solidification (DS) of pseudo-binary alloys Ni–43Al–9.7Cr and Ni–48.3Al–1W led to improvements in both 0.2% compressive yield strength (CYS) and ductility as compared to the single-phase NiAl, with tungsten alloying yielding the greatest strength improvements at room temperature. The room temperature (300 K) CYS of DS NiAl(W) (623 MPa) is larger than the CYS of DS NiAl(Cr) (565 MPa) and DS NiAl (435 MPa). The CYS of the three alloys dropped with increasing test temperature, and at 800 K, the CYS values for the three materials were comparable (356, 315 and 344 MPa for NiAl, NiAl(W) and NiAl(Cr), respectively). All the DS alloys exhibited greater than near-zero ductility of polycrystalline β-NiAl at room temperature, with the fracture strain being the largest for the DS NiAl(Cr) (16.6%), followed by DS NiAl(W) (9.8%) and DS NiAl (7.33%). At room temperature, the DS NiAl(W) shows transgranular failure, the NiAl(Cr) shows a mixed mode failure (predominantly intergranular), whereas β-NiAl shows intergranular failure. The strength and ductility data, and fractography suggest that ductile-phase toughening and strengthening by second phases are responsible for the observed improvements in the ductility and strength. Limited tensile tests on the DS NiAl and DS NiAl(Cr) indicate a Bauschinger-like effect in that the CYS is greater than the tensile yield strength.
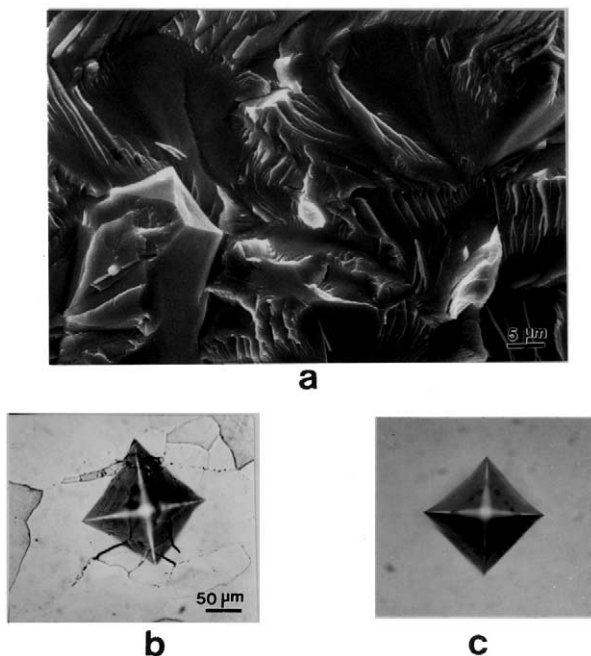
Fig. 9. (a) Fracture surface of a DS Ni–46Al specimen tested for its modulus of rupture (MOR) at room temperature using a four-point bend test, and (b) and (c) show micro-indentations produced using a diamond pyramid indentor in (b) a powder-processed NiAl specimen and (c) a DS NiAl specimen that utilized the powder processed material as a feedstock for the directional solidification.

References

[1] J.D. Cotton, R.D. Noebe, M.J. Kaufmann, Intermetallics 1 (1993) 3.
[2] J.D. Destefani, Adv. Mater. Process. 2 (1989) 37.
[3] R. Darolia, D. Lahrman, R. Field, Scr. Metall. 26 (1992) 1007.
[4] K.S. Kumar, S.K. Mannan, R.K. Viswanadham, Acta Metall. Mater. 40 (6) (1992) 1201.
[5] S.N. Tewari, NASA Technical Note D-8355, 1977.
[6] R.D. Noebe, A. Misra, R. Gibala, ISIJ Int. 31 (10) (1991) 1172.
[7] D.R. Pank, M.V. Nathal, D.A. Koss, J. Mater. Res. 5 (1990) 942.
[8] K. Ishida, R. Kainuma, N. Ueno, T. Nishizawa, Metall. Trans. 22A (1991) 441.
[9] S. Guha, P.R. Munroe, I. Baker, MRS Symp. Proc. 133 (1989) 633.
[10] F.E. Heredia, M.Y. He, G.E. Lucas, A.G. Evans, H.E. Deve, D. Konitzer, Acta Metall. 41 (2) (1993) 505.
[11] J. Kluver, G. Sauthoff, Z. Metallkde. 83 (1992) 699.
[12] X.F. Chen, D.R. Johnson, B.F. Oliver, Scr. Metall. Mater. 30 (8) (1994) 975.
[13] D.R. Johnson, S.M. Joslin, B.F. Oliver, R.D. Noebe, J.D. Whittenberger, in: D. Miracle, J. Graves, D. Anton (Eds.), Intermetallic-Matrix Composites II. In: Materials Research Society Symposium Proceedings, vol. 273, Materials Research Society, 1992, p. 87.
[14] T. Hirano, T. Mawari, in: R. Darolia, J.J. Lewandowski, C.T. Liu, P.L. Martin, D.B. Miracle, M.V. Nathal (Eds.), Structural Intermetallics, TMS, 1993, p. 437.
[15] J.L. Walter, H.E. Cline, Metall. Trans. 1 (1970) 1221.
[16] W.S. Waltson, R.D. Field, J.R. Dobbs, D.F. Lahrman, R. Darolia, in: R. Darolia, J.J. Lewandowski, C.T. Liu, P.L. Martin, D.B. Miracle, M.V. Nathal (Eds.), Structural Intermetallics, TMS, 1993, p. 523.
[17] R. Tiwari, S.N. Tewari, R. Asthana, A. Garg, J. Mater. Sci. 30 (1995) 4861.
[18] R. Tiwari, S.N. Tewari, R. Asthana, A. Garg, Mater. Sci. Eng. A192/193 (1995) 356.

[19] R.D. Field, D.F. Lahrman, R. Darolia, Acta Metall. Mater. 39 (12) (1991) 2961.

[20] M. Dollar, S. Dymek, S.J. Hwang, P. Nash, Metall. Trans. 24A (1993) 1993.

[21] G. Sauthoff, in: R. Darolia, J.J. Lewandowski, C.T. Liu, P.L. Martin, D.B. Miracle, M.V. Nathal (Eds.), Structural Inter-metallics, TMS, 1993, p. 845.

[22] R.R. Bowman, R.D. Noebe, S.V. Raji, I.E. Locci, Metall. Trans. 23A (1992) 1493.

[23] K. Matsugi, D.W. Wenman, N.S. Stoloff, Scr. Metall. 27 (1992) 1633.